A MULTI-MODEL INCREMENTAL ADAPTIVE STRATEGY TO ACCELERATE PARTITIONED FLUID-STRUCTURE ALGORITHMS USING SPACE-MAPPING

Thomas P. Scholcz[*]**, Alexander H. van Zuijlen and Hester Bijl**

[*]Faculty of Aerospace Engineering
Delft University of Technology
Kluyverweg 1, 2629 HS Delft, The Netherlands
e-mail: t.p.scholcz@tudelft.nl

Key words: Fluid-structure interaction, Partitioned coupling, Space-mapping, Multi-fidelity models, Reduced Order Models

Abstract. High fidelity analysis of fluid-structure interaction systems is often too time-consuming when a large number of model evaluations are required. The choice for a solution procedure depends often on the efficiency of the method and the possibility of reusing existing field solvers. Aggressive Space-Mapping, a technique originally developed for multi-fidelity optimization, is applied to accelerate the partitioned solution procedure of a high fidelity fluid-structure interaction model. The method supports software modularity. Aggressive Space-Mapping (ASM) is applied to an academic testcase and the results are compared with the corresponding Incremental Quasi-Newton (IQN) method. An efficiency metric is defined to facilitate the comparison. The ASM method is found to be more efficient than the corresponding IQN method for the testcases considered. The efficiency of space-mapping increases with increasing fluid-to-structure mass ratio, indicating that the method is especially useful for strongly coupled problems.

1 INTRODUCTION

High-fidelity analysis of fluid-structure interaction systems is often too time-consuming when a large number of model evaluations are required. Examples are found in design, optimization and stochastic analysis of fluid-structure interaction systems [1, 2, 4].

The aim of this contribution is to efficiently obtain transient solutions of a high-fidelity model using a partitioned procedure in combination with a technique from multi-fidelity optimization called Aggressive Space-Mapping (ASM) [1]. Using ASM, information of a cheap low-fidelity model is exploited to accelerate the solution procedure of an expensive high-fidelity model. In the following the cheap low fidelity model is named "the coarse model" and the expensive high-fidelity model "the fine model". Coarse models can be categorized as [2]

1. Data-fit models: response surfaces, kriging, radial basis functions etc.

2. Reduced order models: Proper Orthogonal Decomposition, modal analysis, Volterra series etc.

3. Hierarchical models: physics-based models of lower fidelity.

In turn, hierarchical models can be categorized as

1. Low-fidelity models that neglect some physics modeled by the high-fidelity models.

2. Low-fidelity models that are the same as the high fidelity model, but converged to a higher residual tolerance.

3. Low-fidelity models that are the same as the high fidelity model, but discretized on a coarser grid or using a lower order disretization method.

Using defect correction with coarse models in the latter category emanates in a wide range of methods known as multi-grid or coarse-grid methods. The application of coarse-grid methods on a fluid-structure interaction problem has been thoroughly investigated in [3]. The observed efficiency gains of coarse-grid methods motivates to explore the application of other defect correction based algorithms such as space-mapping.

An important distinction can be made in the way coarse models are derived from fine models. For the derivation of a large class of coarse models, detailed preliminary problems need to be solved first. Examples are the classical POD and the Volterra series model reduction methods. This is called the a posteriori approach. The a posteriori approach is useful when the coarse model is able to capture variations in model parameters. In that case, it can be used to replace the fine model in design, optimization or uncertainty analysis. On the other hand, there exist the a priori approach [7] which does not assume prior knowledge of the fine model solution but either starts from a model that was initially derived from the fine model and/or is improved during the solution procedure of the fine model.

The advantage of improving the coarse model and solving the fine model simultaneously is that coarse model information can be used to accelerate the solution procedure of the fine model. Examples of such hybrid strategies are found in [5, 6]. Here, a reduced order model is built up during the coupling iterations of a partitioned (implicit) fluid-structure algorithm. The reduced order model is subsequently used to enhance the convergence of fixed point iterations. Model adaptation is performed by enriching the ROM basis from input-output information of the fine model.

Other techniques use reduced order models to provide a better initial guess for the iterative process at the next time step in an implicit time-integration scheme. Examples are found in [8, 9] . Here, a POD-based ROM is built up during the integration of the fine model. Model adaptation is performed by changing the ROM basis using a so-called

incremental eigenspace algorithm. Typically a ROM-prediction is followed by a fine model correction, if necessary.

In this contribution we aim to explore the application of space-mapping to accelerate the solution procedure of the fine model. Model adaptation is performed via an adaptively improved inverse space-mapping function during the coupling iterations at each time step in a partitioned fluid-structure algorithm. Defect correction on the fluid-structure interface is employed to find the new iterate. Using this strategy, any coarse model could be used that shares the interface degrees of freedom with the fine model. The fine and coarse models are considered "black-boxes" in the space-mapping approach. Similar to the method in [9], the solution of the coarse model can be interpreted as a "shadow" that runs parallel with the solution of the fine model.

First, the general fluid-structure problem is formulated followed by a short discussion of the most common coupling techniques. The concept of space-mapping is explained and the resulting algorithm is applied to a 1-D testcase. Only physics-based models of lower fidelity are used as coarse models in the space-mapping algorithm. Other coarse model types can be used but are not considered in this contribution. Finally, the results are presented and conclusions are drawn.

2 Partitioned coupling techniques

Implicit time integration is often used to ensure a stable numerical scheme. Since implicit schemes require matching conditions at the new time instant t^{n+1}, these schemes lead to coupled problems at each time step in the simulation. Let the vector $\mathbf{v}$ denote the flow variables and vector $\mathbf{u}$ the structure variables at the new time level t^{n+1}. Hiding the dependency on the solution of previous time levels, the coupled problem at time step t^{n+1} is formulated as

$$\mathbf{f}(\mathbf{v}, \mathbf{u}) = \mathbf{0}, \tag{1}$$

$$\mathbf{s}(\mathbf{v}, \mathbf{u}) = \mathbf{0}, \tag{2}$$

where $\mathbf{f}$ represents the discrete fluid equations and $\mathbf{s}$ the discrete structure equations. Solving the discrete fluid equations is often much more expensive than solving the discrete structure equations due to the large range of important scales present in the fluid.

2.1 Problem formulation

The problem can be formulated as a problem in the degrees of freedom of the fluid-structure interface only, with the flow variables $\mathbf{v}$ and structure variables $\mathbf{u}$ treated as internal variables of the residual operator [5, 6]. A Dirichlet-Neumann decomposition is normally employed to solve the system in a partitioned fashion. Introducing the fluid operator $F()$ and structure operator $S()$:

$$\mathbf{y} = F(\mathbf{x}) \qquad\qquad\qquad \mathbf{x} = S(\mathbf{y})$$

1. Apply the interface displacement $\mathbf{x}$ to the boundary of the fluid domain.

2. Deform the grid in the fluid domain to the displacement of the boundary.

3. Calculate the flow variables $\mathbf{v}$ in the fluid domain.

4. Obtain the stress $\mathbf{y}$ on the boundary

1. Apply the stress $\mathbf{y}$ on the boundary of the structure.

2. Calculate the structural variables $\mathbf{u}$ in the domain of the structure.

3. Obtain the displacement $\mathbf{x}$ on the boundary of the structure,

It follows by substitution of $\mathbf{y} = F(\mathbf{x})$ in $\mathbf{x} = S(\mathbf{y})$ that

$$\underbrace{S \circ F(\mathbf{x}) - \mathbf{x}}_{\mathbf{R}(\mathbf{x})} = \mathbf{0}. \tag{3}$$

Strong coupling algorithms aim to minimize residual $\mathbf{R}$ as far as possible using a minimal number of residual evaluations at each time step in the sequential time integration process. The kinematic and dynamic interface conditions at the fluid-structure interface are satisfied when equation (3) holds. For an overview of strong coupling procedures, see [10, 11]. As mentioned in [11], the choice of partitioned approach often depends on the possibility of reusing existing field solvers. The strategy presented in this work supports software modularity and is in addition modular with respect to the coarse models used to accelerate the solution procedure of the fine model.

2.2 Classical coupling algorithms

Classical algorithms aim to reduce residual $\mathbf{R}$ directly without the use of a coarse model space. The most common coupling algorithms in this category that support software modularity are found in [10, 11]. These are: the fixed-point iteration method, fixed-point iteration method with Aitken acceleration and Incremental Quasi-Newton (IQN) methods. Space-mapping is introduced in section 2.3. It is shown in section 2.3.2 that the resulting ASM algorithm is related to the IQN algorithm, which motivates a comparison between the two algorithms. This is done by performing numerical experiments in section 3.

2.3 Space-mapping

Space-mapping relies on the availability of an expensive fine model and a cheap coarse model that model the same physical phenomena. The use of the fluid operator is the most expensive operation in most fluid-structure interaction problems. For this reason we assume the availability of a fine and coarse fluid operator, resulting in the definition of the fine and coarse residual $\mathbf{R}$ and $\tilde{\mathbf{R}}$:

Fine fluid model :

1. Evaluation of $F()$ expensive.

2. Fine residual: $\mathbf{R}(\mathbf{x}) = S \circ F(\mathbf{x}) - \mathbf{x}$

3. Solution: $\mathbf{x}^* = \arg\min ||\mathbf{R}(\mathbf{x})||$

4. Accurate solution.

Coarse fluid model :

1. Evaluation of $\tilde{F}()$ cheap.

2. Coarse residual $\tilde{\mathbf{R}}(\mathbf{z}) = S \circ \tilde{F}(\mathbf{z}) - \mathbf{z}$

3. Solution $\mathbf{z}^* = \arg\min ||\tilde{\mathbf{R}}(\mathbf{z})||$

4. Inaccurate solution.

The solution of the fine and coarse model at t^{n+1} are denoted by $\mathbf{x}^*$ and $\mathbf{z}^*$.

2.3.1 Space-mapping function

Let $\mathbf{X}$ be the space of all interface displacements that can be reached by the fine model and let $\mathbf{Z}$ be all interface displacements that can be reached by the coarse model. The concept of space-mapping is shown in figure 1.
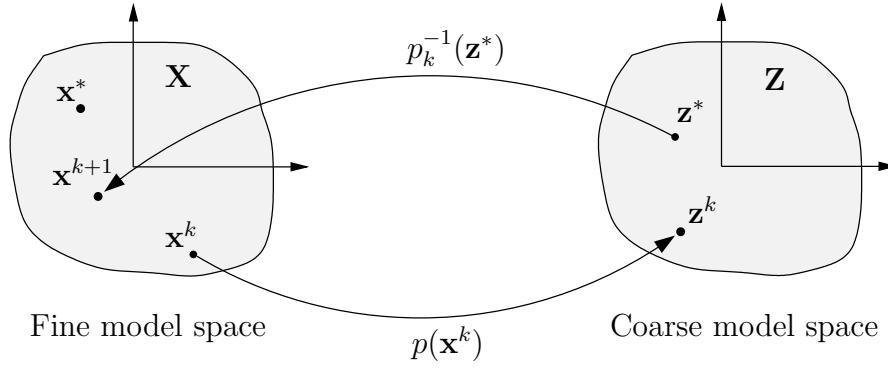

Figure 1: Concept of space-mapping

A choice for the space-mapping function could be

$$\mathbf{z} = p(\mathbf{x}) = \arg\min_{\mathbf{z} \in \mathbf{Z}} ||\tilde{\mathbf{R}}(\mathbf{z}) - \mathbf{R}(\mathbf{x})||, \tag{4}$$

which can be evaluated using coupling iterations with the coarse model, e.g by fixed-point iterations

$$\mathbf{z}^{q+1} = S \circ \tilde{F}(\mathbf{z}^q) - \mathbf{R}(\mathbf{x}). \tag{5}$$

The space-mapping function has the following property:

$$p(\mathbf{x}^*) = \mathbf{z}^*, \tag{6}$$

which states that the mapping function p is perfect [1]. In words: the space-mapping function maps the fine model solution $\mathbf{x}^*$ to the solution of the coarse model, $\mathbf{z}^*$. The inverse of the space-mapping function is given by

$$\mathbf{x} = p^{-1}(\mathbf{z}) = \arg\min_{\mathbf{x} \in \mathbf{X}} ||\mathbf{R}(\mathbf{x}) - \tilde{\mathbf{R}}(\mathbf{z})||. \tag{7}$$

Evaluation of the inverse space-mapping function in (7) is as hard as solving the fine model directly. Therefore, an approximation is used at iterate number k:

$$\mathbf{x}^{k+1} = p_k^{-1}(\mathbf{z}^*) \tag{8}$$

Due to the fact that $p_k^{-1} \approx p^{-1}$ we have $\mathbf{x}^{k+1} \neq \mathbf{x}^*$ but as $p_k \to p^{-1}$ for increasing k it holds that $\mathbf{x}^{k+1} \to \mathbf{x}^*$ upon convergence. When a Taylor series approximation is used for the inverse space-mapping function, the ASM method results. This is the topic of the next section.

2.3.2 Aggressive Space-Mapping method

The space-mapping function is expanded in a Taylor series

$$p_k(\mathbf{x}) \approx p(\mathbf{x}^k) + \nabla_{\mathbf{x}}^k p(\mathbf{x} - \mathbf{x}^k). \tag{9}$$

Using the relations $\mathbf{z}^k = p(\mathbf{x}^k)$ and $\mathbf{z} \approx p_k(\mathbf{x})$, the approximation of the inverse space-mapping function is found from equation (9)

$$p_k^{-1}(\mathbf{z}) \approx \mathbf{x}^k + (\nabla_{\mathbf{x}}^k p)^{-1}(\mathbf{z} - \mathbf{z}^k). \tag{10}$$

The new iterate is found by substitution of the approximated inverse space-mapping function from equation (10) in equation (8)

$$\mathbf{x}^{k+1} = \mathbf{x}^k + (\nabla_{\mathbf{x}}^k p)^{-1}(\mathbf{z}^* - \mathbf{z}^k). \tag{11}$$

The ASM method is summarized in algorithm 1 and compared with the IQN method in algorithm 2. Both algorithms use Broyden's first method to update the Jacobian. Other Jacobian approximations could be used as long as input/output information is sufficient in order to obtain the approximation, e.g. the method of Vierendeels and Degroote [5]. Line number 4 and 15 are left blank in algorithm 2 to emphasize that additional work is performed by the ASM algorithm compared to the IQN algorithm. In addition to the work performed to evaluate the space-mapping functions on line 4 and 15, work need to be performed to obtain the coarse model solution $\mathbf{z}^*$. From the comparison of algorithm 1 and 2 it becomes clear that there is a strong connection between the ASM method and the IQN method. The ASM method reduces to the IQN method when the Taylor expansion of the fine model is taken as the coarse model $\tilde{\mathbf{R}}(\mathbf{z}) = \mathbf{R}^k + \nabla_{\mathbf{x}}^k \mathbf{R}(\mathbf{z} - \mathbf{x}^k)$ in the space mapping procedure. The IQN algorithm is therefore a special case of the ASM algorithm.

On the other hand, we can think of the ASM method as a quasi-Newton method applied to the (nonlinear) system of equations $p(\mathbf{x}) - \mathbf{z}^* = \mathbf{0}$ instead of $\mathbf{R}(\mathbf{x}) = \mathbf{0}$.

Algorithm 1 Aggressive Space-Mapping

1: $k = 0$
2: $\nabla_{\mathbf{x}}^0 p = \mathbf{I}$
3: $\mathbf{R}^0 = S \circ F(\mathbf{x}^0) - \mathbf{x}^0$
4: $\mathbf{z}^0 = \operatorname{argmin}_{\mathbf{z} \in \mathbf{Z}} ||\tilde{\mathbf{R}}(\mathbf{z}) - \mathbf{R}^0||$
5: **while** $||\mathbf{R}^k|| > \epsilon$ **do**
6:   **if** $k = 0$ **then**
7:     $\mathbf{x}^{k+1} = \mathbf{x}^k + (\nabla_{\mathbf{x}}^k p)^{-1}(\mathbf{z}^* - \mathbf{z}^k)$
8:   **else**
9:     $\Delta \mathbf{x} = \mathbf{x}^k - \mathbf{x}^{k-1}$
10:     $\nabla_{\mathbf{x}}^k p = \nabla_{\mathbf{x}}^{k-1} p + \frac{\mathbf{z}^k - \mathbf{z}^{k-1} - \nabla_{\mathbf{x}}^{k-1} p \Delta \mathbf{x}}{\Delta \mathbf{x}^T \Delta \mathbf{x}} \Delta \mathbf{x}^T$
11:     $\mathbf{x}^{k+1} = \mathbf{x}^k + (\nabla_{\mathbf{x}}^k p)^{-1}(\mathbf{z}^* - \mathbf{z}^k)$
12:   **end if**
13:   $k = k + 1$
14:   $\mathbf{R}^k = S \circ F(\mathbf{x}^k) - \mathbf{x}^k$
15:   $\mathbf{z}^k = \operatorname{argmin}_{\mathbf{z} \in \mathbf{Z}} ||\tilde{\mathbf{R}}(\mathbf{z}) - \mathbf{R}^k||$
16: **end while**

Algorithm 2 Incremental Quasi-Newton

1: $k = 0$
2: $\nabla_{\mathbf{x}}^0 \mathbf{R} = -\mathbf{I}$
3: $\mathbf{R}^0 = S \circ F(\mathbf{x}^0) - \mathbf{x}^0$
4:
5: **while** $||\mathbf{R}^k|| > \epsilon$ **do**
6:   **if** $k = 0$ **then**
7:     $\mathbf{x}^{k+1} = \mathbf{x}^k - (\nabla_{\mathbf{x}}^k \mathbf{R})^{-1} \mathbf{R}^k$
8:   **else**
9:     $\Delta \mathbf{x} = \mathbf{x}^k - \mathbf{x}^{k-1}$
10:     $\nabla_{\mathbf{x}}^k \mathbf{R} = \nabla_{\mathbf{x}}^{k-1} \mathbf{R} + \frac{\mathbf{R}^k - \mathbf{R}^{k-1} - \nabla_{\mathbf{x}}^{k-1} \mathbf{R}}{\Delta \mathbf{x}^T \Delta \mathbf{x}} \Delta \mathbf{x}^T$
11:     $\mathbf{x}^{k+1} = \mathbf{x}^k - (\nabla_{\mathbf{x}}^k \mathbf{R})^{-1} \mathbf{R}^k$
12:   **end if**
13:   $k = k + 1$
14:   $\mathbf{R}^k = S \circ F(\mathbf{x}^k) - \mathbf{x}^k$
15:
16: **end while**

More computational work per fine model evaluation is performed in the ASM algorithm than in the IQN algorithm. The number of fine residual evaluations should therefore decrease significantly to gain efficiency with respect to the IQN method. The efficiency of the ASM method depends on the kind of coarse model used, the alignment of the coarse and fine model in time and model parameters. For a certain choice of coarse model, the efficiency should be determined by performing numerical experiments. To ease comparison of different techniques, an efficiency metric is defined in the following section.

2.4 Aggressive Space-Mapping versus Incremental Quasi-Newton method

The efficiency of the ASM method and the IQN method is determined by the cost per time step for a fixed tolerance ϵ in algorithm 1 and 2. Let $W_f^{k,n}$ and $W_c^{k,n}$ be the cost (flops or CPU time) of the kth fine and coarse model iteration respectively at the nth time step in the sequential time integration process.

$$W_{\text{f}}^{k,n} = \text{CPU time} \quad S \circ F(\mathbf{x}^k) - \mathbf{x}^k, \tag{12}$$
$$W_{\text{c}}^{k,n} = \text{CPU time} \quad S \circ \tilde{F}(\mathbf{z}^k) - \mathbf{z}^k. \tag{13}$$

The average cost per time step t^n of a fine and coarse model residual evaluation is then found from

$$\bar{W}_{\mathrm{f}}(t^n) = \frac{1}{N_{\mathrm{f}}} \sum_{k=1}^{k=N_{\mathrm{f}}} W_{\mathrm{f}}^{k,n} \quad \text{and} \quad \bar{W}_{\mathrm{c}}(t^n) = \frac{1}{N_{\mathrm{c}}} \sum_{k=1}^{k=N_{\mathrm{c}}} W_{\mathrm{c}}^{k,n} \tag{14}$$

The total cost per time step t^n of the ASM method and the IQN method is then estimated by

$$W^{\mathrm{sm}}(t^n) = \bar{W}_f^{\mathrm{sm}} N_f^{\mathrm{sm}} + \bar{W}_c^{\mathrm{sm}} N_c^{\mathrm{sm}} \quad \text{and} \quad W^{\mathrm{qn}}(t^n) = \bar{W}_f^{\mathrm{qn}} N_f^{\mathrm{qn}}, \tag{15}$$

where $\bar{W}_f^{\mathrm{sm}}$ and $\bar{W}_f^{qn}$ are the average work of fine model residual evaluations per time step in the ASM and IQN method respectively. The time dependent efficiency of the ASM algorithm relative to the IQN algorithm is subsequently found from the ratio of work per time step

$$\eta(t^n) = 1 - \frac{W^{\mathrm{sm}}(t^n)}{W^{\mathrm{qn}}(t^n)} = 1 - \underbrace{\frac{N_f^{\mathrm{sm}}}{N_f^{\mathrm{qn}}}}_{\kappa_f} - \underbrace{\frac{\bar{W}_c^{\mathrm{sm}}}{\bar{W}_f^{\mathrm{qn}}}}_{\gamma_c} \underbrace{\frac{N_c^{sp}}{N_f^{qn}}}_{\kappa_c}. \tag{16}$$

Equation (16) is valid since $\bar{W}_f^{sm} \approx \bar{W}_f^{qn}$. The relative efficiency at t^n depends on three ratios: the ratio of fine model residual evaluations κ_f, the ratio of coarse to fine work γ_c and the ratio of the coarse to fine residual evaluations κ_c. The ASM method is more efficient than the IQN method if $\eta > 0$. From (16) it becomes clear that the success of space-mapping is not only determined by the reduction of fine model evaluations but also by the cost to achieve this reduction. For a constant κ_f, the product $\gamma_c \kappa_c$ determines the effect on the relative efficiency. It follows that a large number of coarse model evaluations with a very cheap coarse model can be as successful as a few iterations with a more expensive coarse model as long as the same reduction in the number of fine model evaluations is achieved.
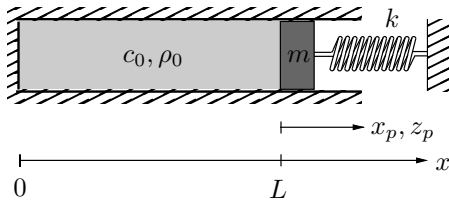
3   1-D test case: Piston problem

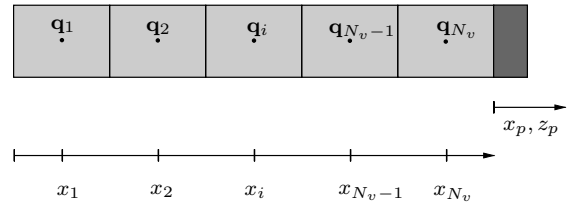**Figure 2**: 1D testcase: Conceptual domain

Figure 3: 1D testcase: Computational domain

3.1   Fine fluid model

The fluid in the piston is governed by the Euler equations of gas dynamics [3, 12]

$$\partial_t \mathbf{q} + \partial_x \mathbf{f}(\mathbf{q}) = \mathbf{0}. \tag{17}$$

Since a one-dimensional compressible inviscid fluid is assumed with $p = \frac{p_0}{\rho_0^\gamma} \rho^\gamma$, the energy equation in (17) becomes redundant and only the mass and momentum balance are necessary to describe the physics of the fluid. The state and flux vector are therefore given by

$$\mathbf{q} = (\rho \ \rho u)^T \quad \text{and} \quad \mathbf{f}(\mathbf{q}) = (\rho u \ \rho u^2 + p)^T, \tag{18}$$

with ρ the fluid density and u the horizontal fluid velocity. The Finite Volume technique is used to transform the integral form of equation (17) to a semi-discrete nonlinear system of equations

$$\partial_t \mathbf{w}_f + \mathbf{A}(\mathbf{w}_f)\mathbf{w}_f + \mathbf{A}_{fs}\mathbf{w}_s = \mathbf{0}. \tag{19}$$

Here, $\mathbf{w}_f = (\mathbf{q}_1^T \ \mathbf{q}_2^T ... \mathbf{q}_{N_v}^T)^T$ is the discrete state vector of the fluid, $\mathbf{A}_{fs}$ is the structure-to-fluid coupling matrix and $\mathbf{w}_s = [x_p \ \dot{x}_p]^T$ the state vector of the structure. The computational domain is shown in figure 3. To perform the coupling, a transpiration boundary condition is used on the fluid-structure interface, see [3]. From (19) it becomes clear that a fine model residual evaluation requires the solution of a nonlinear system of equations. The nonlinear system of equations is solved using simple Picard-iterations.

3.2   Coarse fluid model

If the flux vector $\mathbf{f}$ in (18) is linearized around the equilibrium state of the fluid: $\mathbf{q} = (\rho_0 \ 0)^T$ we obtain

$$\partial_t \mathbf{q}' + \partial_\mathbf{q}\mathbf{f}|_{\mathbf{q}=\mathbf{q}_0} \ \partial_x \mathbf{q}' = \mathbf{0}, \tag{20}$$

with $\partial_\mathbf{q}\mathbf{f}$ the Jacobian of the nonlinear flux $\mathbf{f}$ as found in [3, 12] and $\mathbf{q}'$ a perturbation with respect to the equilibrium state vector $\mathbf{q}_0$. If the Finite Volume method is applied to the integral form of (20), a discrete linear system of equations results

$$\partial_t \mathbf{w}_f' + \mathbf{A}\mathbf{w}_f' + \mathbf{A}_{fs}\tilde{\mathbf{w}}_s = \mathbf{0}. \tag{21}$$

Here, the state vector is denoted $\tilde{w}_s = [z_p \ \dot{z}_p]^T$. A coarse residual evaluation requires only the solution of a linear system of equations.

3.3   Testcases

The fluid-to-structure mass ratio ζ and ratio of characteristic time-scales λ are defined by

$$\zeta = \rho_0 L/m \quad \text{and} \quad \lambda = L\omega/c_0, \tag{22}$$

with $\omega = \sqrt{\frac{k}{m}}$ the natural frequency of the mass-spring system. It is well known that the convergence of fixed-point iterations depends on the ratio $\zeta/\lambda = \frac{\rho_0 c_0}{\sqrt{km}}$ and the time step used in the sequential integration process, see [12]. In order to study the performance of the ASM-algorithm for various levels of coupling strength, we fix the ratio of characteristic time scales and increase the fluid-to-structure mass ratio.

	Similarity parameters		Structural parameters		Fluid parameters		
	$\zeta\;[-]$	$\lambda\;[-]$	$m[kg]$	$k\;[\frac{kg}{ms^2}]$	$L[m]$	$\rho_0[\frac{kg}{m^3}]$	$c_0[\frac{m}{s}]$
FSI-1	1/2	0.85	4	64300	2	1	300
FSI-2	2/3	0.85	3	48225	2	1	300
FSI-3	2	0.85	1	16075	2	1	300

Table 1: Physical parameters and similarity parameters of the 1-D FSI test cases

The testcases are collected in table 1. For each testcase we are interested in the relative time-dependent efficiency η as defined in section 2.4. The coarse fluid-structure model has a (non-dimensional) coupled period of $P_1 = 6.19$, $P_2 = 5.96$ and $P_3 = 5.04$ for the testcases FSI-1, FSI-2 and FSI-3 respectively. Time steps in the simulation are given with respect to the coarse coupled period as will become clear in section 3.4.

3.4 Numerical experiments

The initial conditions and numerical parameters are collected in table 2. The piston is released from an initial displacement. For the nondimensionalization the same convention is used as in [3]. The coarse and fine model use the same discretization.

Description	fine model		coarse model	
Initial piston displacement	$\bar{x}_p^0$	0.5	$\bar{z}_p^0$	0.5
Initial fluid density	$\bar{\rho}^0$	$\frac{2}{3}$	$\bar{\rho}'^0$	$-\frac{1}{3}$
Number of finite volume cells	N_v	64	N_v	64
Number of time steps	N_t	500	N_t	500
Time step	Δt	$P/500$	Δt	$P/500$

Table 2: Nondimensional initial conditions and numerical parameters

The BDF2 time-integration scheme is used to integrate the semi-discrete coupled system in a partitioned way. The tolerance in algorithm 1 and 2 is set to a small value: $\epsilon = 1 \times 10^{-12}$, resulting in a strongly coupled solution. The fine and coarse model fluid density as a function of (nondimensional) space and time is given in figure 4 and 5 respectively for testcase FSI-2. A pressure wave is present in the fine model density response, hitting the piston at $\bar{t}/P_2 \approx 0.4$ and $\bar{t}/P_2 \approx 0.7$. The effect of the pressure wave is also present in

the solution of the piston in figure 6. There is no pressure wave present in the solution of the linear coarse model as can be seen in figure 5 and 7 respectively.
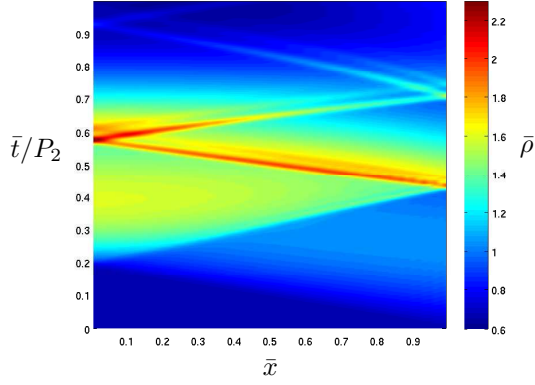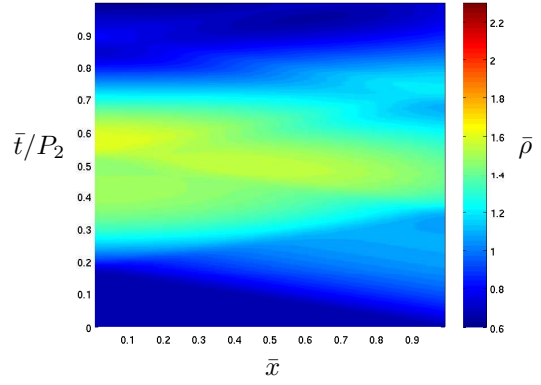

Figure 4: Fine density response of FSI-2

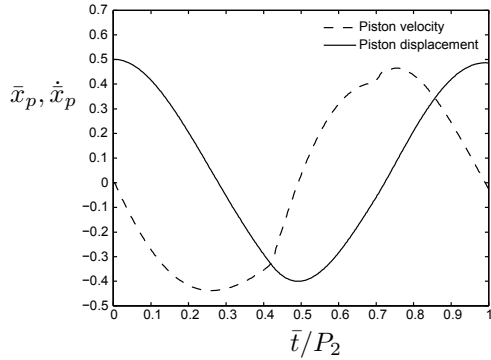**Figure 5**: Coarse density response of FSI-2
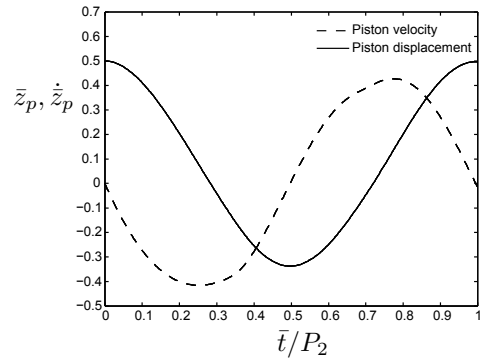

Figure 6: Fine piston response of FSI-2

Figure 7: Coarse piston response of FSI-2

The number of fine model iterations used in the ASM method, the IQN method and the fixed-point iteration method as a function of time are plotted in figure 8. As expected, both ASM and IQN are more efficient than the fixed-point iteration method. The time dependent efficiency of the ASM algorithm relative to the IQN algorithm is shown in figure 9. It can be seen from figure 9 that the efficiency of ASM and IQN are comparable ($\eta \approx 0$), except at the moments when the pressure wave hits the piston. The ASM method is more efficient than the IQN method at these instances. This indicates that the efficiency of ASM increases when a strong interaction between the structure and the fluid is present. The efficiency η is equal to a small negative number $-\gamma_c \kappa_c$ ($O(10^{-3})$) when $N_f^{sm} = N_f^{qn}$. Hence, the coarse model work is negligible for this particular problem. The total relative efficiency of a single period is given by $\hat{\eta} = 1 - \frac{\sum W^{sm}(t^n)}{\sum W^{qn}(t^n)}$. The total efficiencies are

$\hat{\eta}_1 = 6.1\%$, $\hat{\eta}_2 = 6.2\%$ and $\hat{\eta}_3 = 8.3\%$ for FSI-1, FSI-2 and FSI-3 respectively. Hence, the relative efficiency increases when the algorithm is applied to strongly coupled fluid-structure interaction problems.
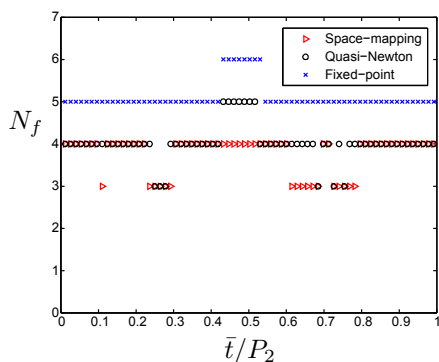

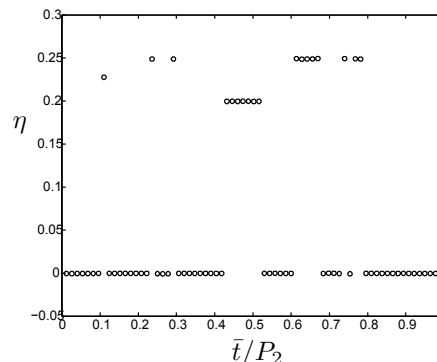**Figure 8**: Fine model iterations N_f for FSI-2

Figure 9: Efficiency η for FSI-2

4 Conclusions

- Aggressive Space-Mapping is successfully applied to obtain the transient solution of an academic fluid-structure problem in a partitioned way.

- Aggressive Space-Mapping is found to be more efficient ($\hat{\eta} = 6\%$ to 8%) than the corresponding Incremental Quasi-Newton method for the considered testcases and time intervals. The time-dependent efficiency is high at the moments of strong interaction ($\eta = 20\%$ to 25%), e.g. when a pressure wave hits the structure.

- The efficiency of Aggressive Space-Mapping increases with increasing fluid-to-structure mass ratio, keeping the ratio of characteristic time scales fixed. The efficiency is therefore higher for strongly coupled problems with large fluid densities and/or flexible and light structures.

5 Acknowledgement

REFERENCES

[1] Echeverría, D. and Hemker, P.W. Space-mapping and defect correction, *CMAM J*(2005) **5**(2):107-136.

[2] Robinson, T.D. and Eldred, M.S. and Willcox K.E. and Haimes, R. Surrogate-based optimization using multifidelity models with variable parameterization and corrected space mapping *AIAA J* (2008) **46**(11):2814–2822

[3] Zuijlen, A.H. and Bosscher, S. and Bijl, H. Two level algorithms for partitioned fluid-structure interaction computations *Comput. Methods Appl. Mech. Engrg.* (2007) **196**(8):1458–1470

[4] Verhoosel, C.V. and Scholcz, T.P. Uncertainty and reliability analysis of fluid-structure stability boundaries, *AIAA J* (2009) **47**(1):91–104.

[5] Degroote, J. and Bathe, K. and Vierendeels, J. Performance of a new partitioned procedure versus a monolithic procedure in fluid-structure interaction *Computers and Structures* (2009) **87**:793–801

[6] Vierendeels, J and Lanoye, L. and Degroote, J. and Verdonk, P Implicit coupling of partitioned fluid-structure interaction problems with reduced order models *Computers and Structures* (2007) **85**:970–976

[7] Ryckelynck, D. and Chinesta, F. On the *a priori* Model Reduction: Overview and Recent Developments *Arch. Comput. Meth. Engng.* (2006) **13**(1):91–128

[8] Ryckelynck, D. and Missoum Benziane, D. Multi-level a priori hyper reduction of mechanical models involving internal variables *Comput. Methods Appl. Mech. Engrg.* (2010) **199**:1134–1142

[9] Markovinović, R. and Jansen, J.D. Accelerating iterative methods using reduced-order models as solution predictors *Int. J. Numer. Methods Engrg.* (2006) **68**:525–541

[10] Matthies, H.G. and Niekamp, R. and Steindorf, J. Algorithms for strong coupling procedures *Comput. Methods Appl. Mech. Engrg.* (2006) **195**:2028–2049

[11] Gallinger, T and Bletzinger, K Comparison of algorithms for strongly coupled partitioned fluid-structure interaction *ECCOMAS* Lisbon, June 2010

[12] Brummelen, E.H. and R. de Borst On the nonnormality of subiteration for a fluid-structure-interaction problem *SIAM J. Sci. Comput.* (2005) **2**:599–621